URB-Solar: An open-source tool for Solar Power Prediction in Urban Areas

Venugopalan S. G. Raghavan
Fluid Dynamics Department
Institute of High Performance Computing
1 Fusionopolis Way
#16-16 Connexis
Singapore 138632

Harish Gopalan*
Fluid Dynamics Department
Institute of High Performance Computing
1 Fusionopolis Way
#16-16 Connexis
Singapore 138632

ABSTRACT

The accurate prediction of the direct and diffuse solar radiation is of foremost importance for deployment of photovoltaic systems. A number of solar radiation forecasting techniques have been developed for longer and shorter forecasting times. Numerical weather prediction (NWP) models provide the best results for the longer forecasting times (4-6 hours), required by utility companies. However, NWP methods are usually developed for clear-sky and open areas. These methods cannot be directly applied to urban areas with shading, trees, multi-surface reflection and other sources of solar radiation losses. To overcome these issues, improvement to existing prediction tools are required. In this study, we develop an automated radiation forecasting tool for urban areas. This tool combines a numerical weather prediction model (Weather Research and Forecasting model) and a solar calculator (developed in the numerical toolbox OpenFOAM) to compute shading, reflection and other losses in the urban canopy. An algorithm for extraction of building outlines, and heights (if they are publicly available) is also developed as a part of the tool. Finally, the coupled solar power estimator can be applied to past, present, or future solar power predictions. Initial results obtained using the developed tool are demonstrated for an urban neighborhood in Singapore.

1 Introduction

The deployment of photovoltaic (PV) systems has been growing at a rapid pace around the world. A recently released study [1] has suggested that solar power will generate 20% of global electricity by

*Corrsponding Author: Scientist, Fluid Dynamics Department, Institute of High Performance Computing, 1 Fusionopolis Way, #16-16 Connexis, Singapore 138632, Email:gopalanh@ihpc.a-star.edu.sg

2027. A recent report by National Renewable Energy Lab [2] has shown that the cost of solar system deployment in residential and commercial areas has decreased by at least 4 times from 2010 to 2017. The cost reduction coupled with the improved efficiency of solar panels will further enhance the adoption of solar energy.

The output of a PV system is calculated from the global horizontal irradiance (GHI). Consequently, the accurate assessment of global horizontal irradiance (GHI) is one of the most important parameters to be considered for the deployment of PV systems. GHI forecasting can be performed using statistical [3, 4, 5, 6, 7], cloud imagery and satellite-based [8, 9, 10, 11], and numerical weather prediction (NWP) [11, 12, 13] methods. A discussion of the merits of each of the methods can be found in Ref. [14].

The different forecasting techniques provide the best results for a certain time range. For example, cloud imagery and satellite-based methods show a good performance for a temporal range of 30 minutes to 6 hours [8] while NWP models provide the best results for longer time intervals (more than 4 hours [12]). As a result, hybrid models [3, 15, 16, 17, 18] have been proposed to combine the advantages of the existing methods. The hybrid method combines the radiation forecast from the existing methods to provide a final value. The coupling can be a simple linear or complex non-linear model. These methods are more recent and further verification studies are required to demonstrate its advantages.

In this study, an automated hybrid approach is proposed for the calculation of the GHI in densely packed urban areas. The approach is performed in two-stages: (i) building footprint extraction and (ii) solar power computation. In the first stage, online maps are used to extract the footprint of buildings and location of trees. The buildings and trees are extruded using available information and pictures. It should be noted that this step is not essential for the calculation of the solar power. In the second stage, the solar power is computed in the region of interest. The initial guess for the GHI is calculated using the numerical weather prediction tool Weather Research and Forecasting (WRF) [19] model. However, the detailed three-dimensional canopy information cannot be represented in WRF. So the direct and diffuse solar radiation from WRF is used to drive a solar calculator in the open-source numerical toolbox OpenFOAM [20]. This solar calculator can account for shading, reflection and other losses in the urban canopy.

2 URB-Solar

The proposed tool can be divided into three parts: (i) building and tree extrusion, (ii) numerical weather prediction and (iii) urban solar load calculator. The details of each of these components will be discussed in the current section.

2.1 Building Geometry Creation Algorithm

The flowchart of the building geometry creation algorithm is shown in Fig. 1. In order to obtain the geometry of the buildings, snapshots from resources like Google Maps or onemap were used. Buildings are shown in plan view in such images (see Fig. 2). Color rules are used to get the footprint of the building. In the case of images from onemap, the buildings are typically color coded according to type. Thus from an image, based on the desired type (and thus color), the pixels corresponding to a set of buildings can be extracted. Note that the step of the process where the color type to be used for extraction has to be specified manually. We hope to automate this task in future. Thus for each cluster, manual input is required to provide information on what to look for and extract.

The code that was written to extract pixels corresponding to building outlines has default values corresponding to the generic housing buildings as seen in onemap. For other cases, the user will need to specify the upper and lower bounds (threshold values) of the three color channels - red, green and blue - in order to enable the code to extract out the pixels pertaining to the building outline. Consequently, the code can be used in a wide variety of scenarios as long as the relevant user input for colors is given.

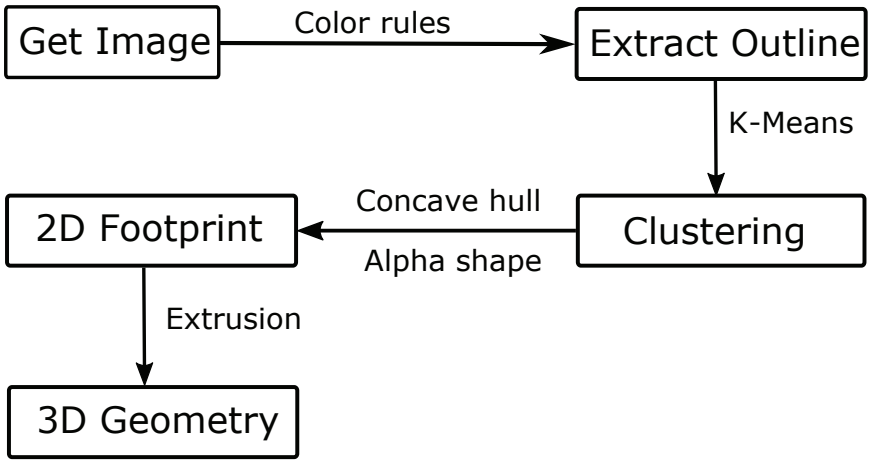

Fig. 1: Flowchart of work flow for the building geometry creation algorithm

Once the process of extracting the pixels is complete, the next step is performed. For an image with multiple buildings, this involves grouping pixels into clusters such that each cluster ideally represents a single building. To perform this, the unsupervised learning technique of k-means clustering [21] was used with the aid of the scikit-learn library in Python [22]. As the goal is to keep user intervention to a minimum, automated rules based on maximum silhouette score [23] are used to decide the number of clusters in the obtained image.

Once the process of grouping is completed, the next step is performed. In this stage, the pixels, which are each individual and discrete particles or points, have to be converted to a continuous representation in order to obtain surfaces. Essentially this involves fitting a shape to the pixels - ordering the points in a particular manner to obtain a building outline (and with it the inner surface as well).

The simplest method of ordering points is to get the convex hull of the points. By definition, a convex hull of a set of points is the smallest enclosed shape that contains all the points in the set [24]. This method is best suited when the resulting shape is expected to be convex. However, the vast majority of the building shapes, at least in Singapore, correspond to more than just simple convex shapes (like rectangles and squares) and consequently, the convex hull algorithm cannot be used. The other limitation with the convex hull approach for shape determination is that it has the tendency to smear and spread the shape out often resulting in greatly distorted (from expected) shape of the geometry.

Consequently, the concave hull algorithm (also called alpha shape algorithm) [25] was used in order to obtain the ordering of the points to create the surface of the building. The implementation involved

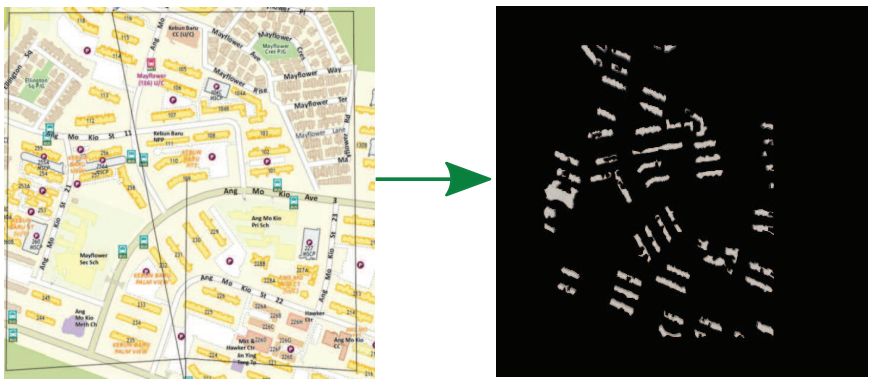

Fig. 2: Extraction of the building footprint from onemap images. All the yellow colored buildings have been extracted.

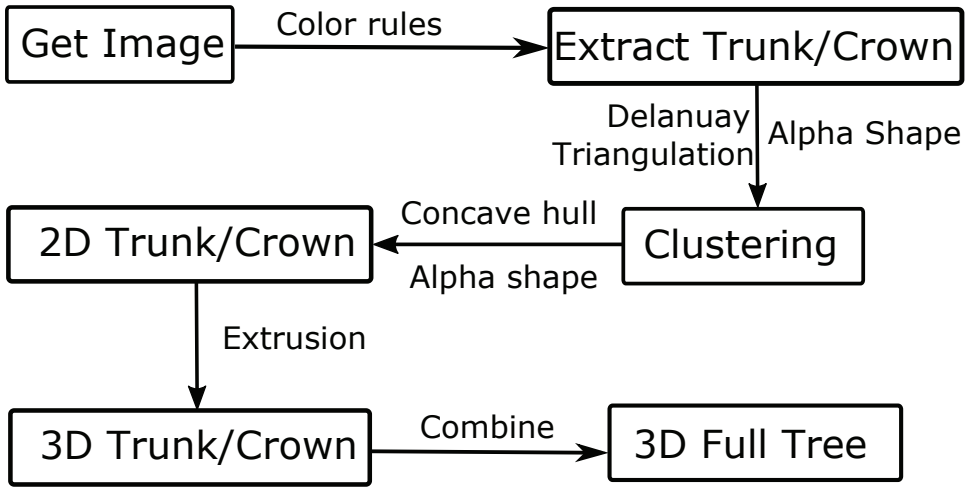

Fig. 3: Flowchart of work flow for the tree extrusion or revolution algorithm

the use of a library for the Concave Hull available online. This library automatically determines the minimal number of points required to define the shape (starts from 3 points and then increases the number of points involved in the computation of the alpha shape).

Once the number of points, as well as the ordering of the points, have been obtained from the concave hull operation, the surface needs to be created. While this can be performed in a variety of ways, in the current work, the Visualization Toolkit (VTK) developed by Kitware (www.vtk.org) is used. Since all the relevant information is already present - vertices and their ordering - the process of creating a polygonal cell in VTK can be performed in a straightforward manner.

The created polygonal cell is then triangulated. This is achieved again by filters within the VTK framework. Triangulating the polygonal cell will aid in writing out the final STL file that is required for the simulations. It is also required in order to perform extrusions on the created polygonal cell.

The cell representing the building footprint is then scaled (after triangulation) depending on the scale of the image. As this information is not evident from the image used to generate the building geometry, it would need to be provided by the user. Based on this information, the triangulated polygonal cell can be extruded, again using the functionality of the VTK class to the desired height. The final solid model created from the method is shown in Fig. 2.

2.2 Tree Geometry

The approach used for the trees was slightly different (see Fig. 3). In the case of the trees, the image was again scanned for pixels belonging to a certain color range (see Fig. 4). However, instead of fitting a concave hull, the Delaunay triangulation filter in VTK was used to directly create the surface. It is possible to use the same method as for the buildings. However, as other methods were being explored, the Delaunay triangulation approach was tested and utilized in this scenario. Thus two sets of geometry were created - one for the trunk and one for the leaves. This geometry is still two-dimensional. In order to convert this to 3D, two methods were explored - a) treating the trunk and leaves of the 2D model as the cross-section of a solid obtained by revolution, or b) treating the trunk and leaves of the 2D model as the cross-section of a solid obtained by extrusion. Both approaches can be employed. The calculations presented in the next section used the revolution based approach.

2.3 Numerical Weather Prediction

The open-source numerical weather prediction model WRF [19] (version 3.9) was chosen to calculate the GHI in the region of interest. WRF can be run as a regional climate model (RCM) or global

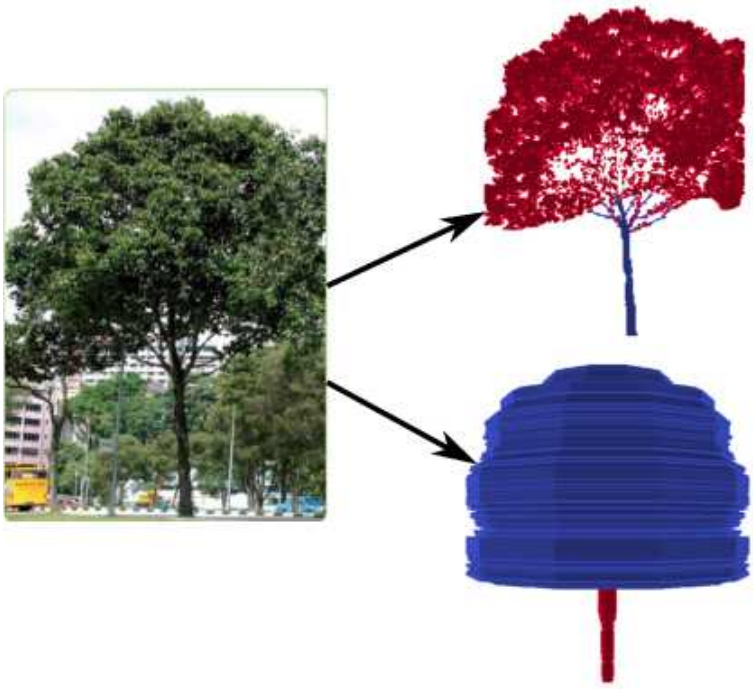

Fig. 4: Creation of the CAD model of the tree from an image (Source: www.nparks.gov.sg). The algorithm creates a two-dimensional representation of the tree. Extrusion or rotation of the two-dimensional object produces the three-dimensional tree model.

climate model (for future weather predictions). The coupling between the results and the solar calculator use the same method for both the modes (regional or global). To speed-up the computations, WRF is run in RCM mode. RCM runs of WRF require lateral boundary conditions to drive the simulations. The datasets provided by the NCEP FNL Operational Model [26] is used to provide the lateral boundary conditions. Additionally, the user has to choose the physics options for running the model. The WRF runs are performed with the following physics options:

1. Microphysics: Thompson aerosol-aware [27]
2. Cumulus parametrization: Grell-Freitas (GF) scheme [28]
3. Short-wave and long-wave radiation: Rapid Radiative Transfer Model for General Circulation Models (RRTMG) scheme [29]
4. Planetary boundary layer: Yonsei University scheme with topography correction for wind-speed [30, 31]
5. Land surface model (LSM): Noah - Multiparameterization (MP) [32, 33]

Four levels of grid nesting are used for performing the simulations. The grids have horizontal resolutions of 27×27 (grid G1) , 9×9 (grid G2), 3×3 (grid G3) and 1×1 (grid G4) km, respectively. In the vertical direction, 48 levels are used and 10 levels are placed within the planetary boundary layer. Solar radiation computations are performed every 5 minutes to provide more detailed GHI values. The code has also been modified to include the enhancements available within WRF-Solar [34]. The time-series output option in WRF is used to provide the radiation values at every time step for a number of grid points. The direct and diffuse solar radiation information from the time-series data is interpolated and used as input for the solar calculator. Numerical details of the procedure will be provided in the next section.

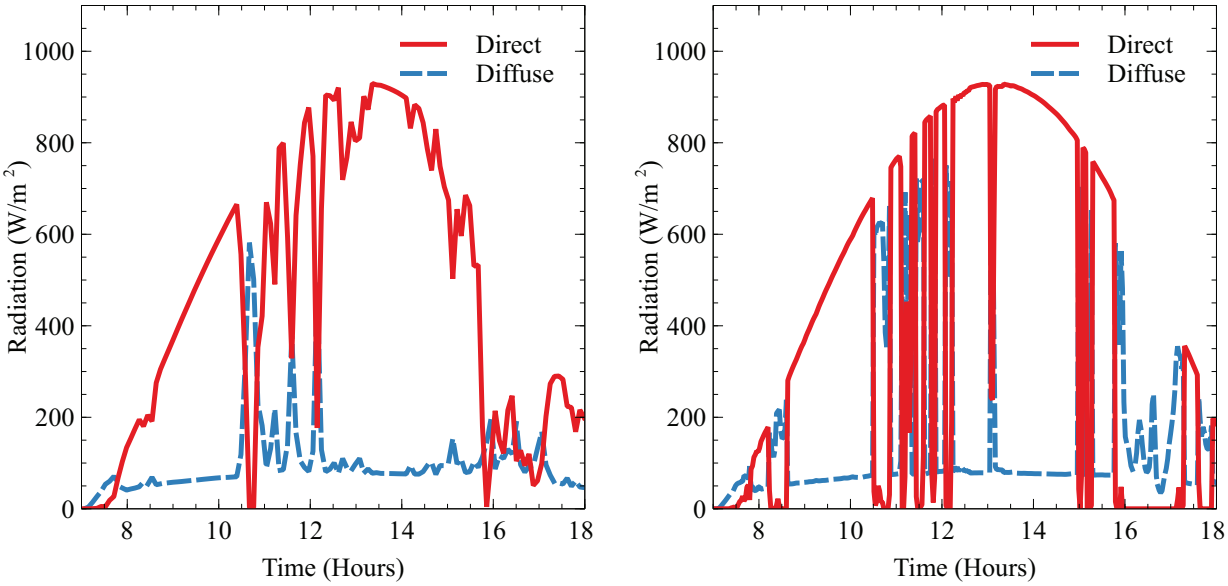

(a) 3×3 km horizontal resolution

(b) 1×1 km horizontal resolution

Fig. 5: Comparison of direct and diffuse solar radiation (as a function of time) on different domains in WRF for Toa Payoh on August 24^{th} ,2017. Simulations in the 1×1 km grid is nested within 3×3 km grid. X-axis represents the hour of the day (in a 0-24 scale) .

2.4 Urban Solar Load Calculator

Urban areas are represented as roughness elements in WRF. As a result, the solar radiation losses in the urban areas due to shading, reflection, etc. cannot be accounted. Solar load calculator is a commonly used computational tool to account for these losses. This method does not include the effects of the participating medium and requires only a fine surface mesh. The calculator requires the following user-input: (i) latitude and longitude of place interest, (ii) day of the year, (iii) direct and diffuse radiation and (iv) material properties. Based on a ray-tracing algorithm, the solar calculator computes the direct, diffuse, and reflected solar radiation on all the vertical and horizontal surfaces. The effects of surface shading, multi-surface reflection and transmission are included in the calculations. This method can be applied to both man-made and natural surfaces. This allows the calculation of detailed multi-surface reflection buildings and trees.

In this study, OpenFoam-v5.0 [35] was used as the solar calculator and a new solver is created to perform the radiation calculations in the urban area. The baseline solar load calculator module available in OpenFOAM-v1612 [36] (ported to OpenFOAM-v 5.0) was modified to compute the loads on horizontal and vertical surfaces. All inputs except material properties (provided by the user) are taken from WRF. A user-defined library is created in OpenFOAM-v 5.0 to read the input information from WRF and process it for use in OpenFOAM.

In the solar load calculator, the direct solar radiation on any surface is calculated as

$$I_{dir} = I\cos(\theta) \tag{1}$$

where I is the direct normal radiation from WRF and θ is the incidence angle. The diffuse terms are calculated using the model of Klucher [37, 38] to account for the anisotropy of the sky and cloudiness effects using the following expression:

$$I_{dif} = \frac{1}{2} I_{difWRF}[1+\cos(\beta)]M_1 M_2 \tag{2}$$

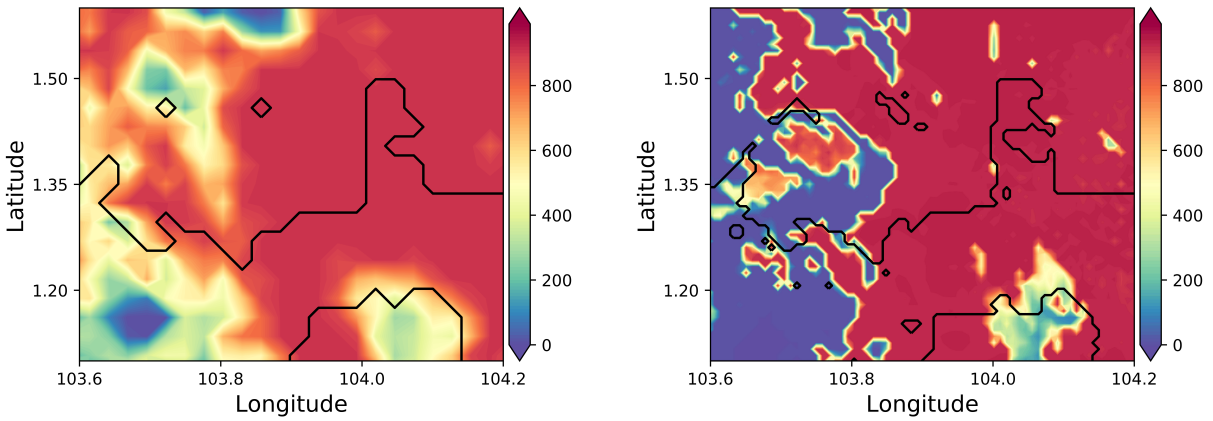

(a) 3×3 km horizontal resolution

(b) 1×1 km horizontal resolution

Fig. 6: Comparison of direct solar radiation (in Wm^{-2}) obtained from WRF simulation at 2 PM (Singapore standard time) on August 24^{th} , 2017.

$$M_1 = 1 + F \sin^3(0.5\beta) \tag{3}$$

$$M_2 = 1 - F \cos^2(\theta) \sin^3(z) \tag{4}$$

$$F = 1 - \left(\frac{I_{difWRF}}{I + I_{difWRF}} \right)^2 \tag{5}$$

where I_{dif} is the diffuse radiation on the horizontal/vertical surface, I_{difWRF} is the diffuse radiation from WRF on a horizontal surface, β is the surface tilt angle, z is the solar zenith angle, and F is a cloudiness function [38]. Next, a face-shading algorithm is used to account for the shading effect due to neighboring buildings and trees. Transmission effects are not included for buildings. A simple algebraic model is used to account for the transmission effects in trees [39]. For closely spaced surfaces, single radiation reflection bounce may not be sufficient. Multi-surface reflections (buildings and trees) are considered diffuse and can be calculated using a view-factor based approach as follows [40]:

$$Q_r^k = -(1 - \alpha_k)(I_{dir} + I_{dif}) + \alpha_k \sum_{j=1}^{N} Q_r^j \tag{6}$$

where Q_r^k is the net radiation flux on any surface after multiple reflections, and α_k is the albedo of the surface. More advanced radiation models, considering the effects of participating medium/specular reflection, can be employed for future studies.

3 Illustration

To illustrate the use of a tool, the residential town of Toa Payoh (1.334° N, 103.856° E) in the central region of Singapore is chosen. WRF simulations are performed for August 23rd and 24th, 2017. These two days were chosen as no rain was observed in the area. The first-day simulation data is used for simulation start-up and not used. The variation of the direct and diffuse solar radiation during day-time of August 24th is shown in Fig. 5a and b for grids G3 and G4. The differences in the radiation pattern

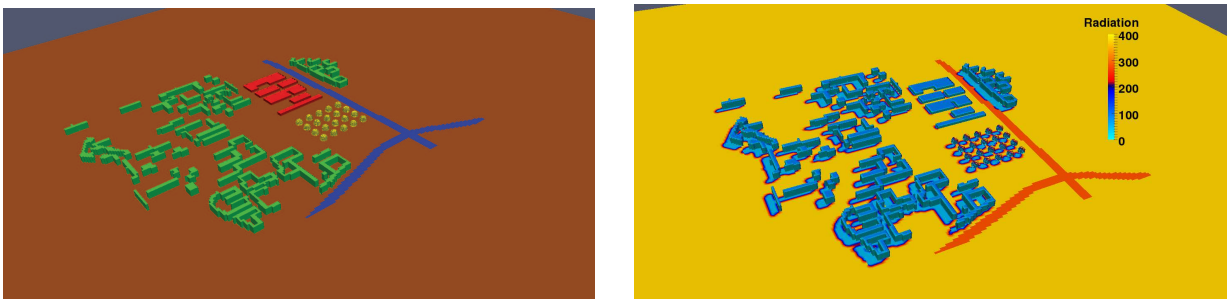

(a) Different materials: green and red - buildings, yellow - trees, blue - expressway, and brown-terrain

(b) Contour plot of solar radiation forecast (in Wm^{-2}) on different surfaces

Fig. 7: Illustration of the solar load calculator

(observed between 10 - 12 PM and 4 - 6 PM) is due to the better cloud resolution in the finer grid G4. The contour plot of the direct solar radiation on both these grids is shown in Fig. 6 for the entire Singapore region (represented approximately with a black-line). The number of grid points used in G3 and G4 is $\sim 20 \times 20$ and $\sim 60 \times 60$, respectively. The line and contour plots emphasis the importance of using a finer grid and better resolving the cloud motion in the climate model. This is essential for PV system operation since the fraction of the direct and diffuse radiation determine the power output from the plant.

Once the WRF simulations are completed, the direct and diffuse solar radiation data shown in Fig. 6b is used to drive the solar calculator simulations. The STL files for performing the solar forecasting are created using the method discussed in Section 2.1. The CAD model is shown in Fig. 7a. Before performing the calculations, albedo values have to be assigned. The albedo value for the terrain (assumed flat) is taken from WRF. The albedo values for buildings, expressways (minor roads, neglected for this study) and trees were chosen to be 0.8, 0.4 and 0.1, respectively [19]. The forecasted solar radiation results are shown at 11 AM in Fig. 7b (direct solar radiation shows a drop due to cloud cover in Fig. 5b). It can be seen that the use of the input from climate model allows the solar calculator to account for rapid

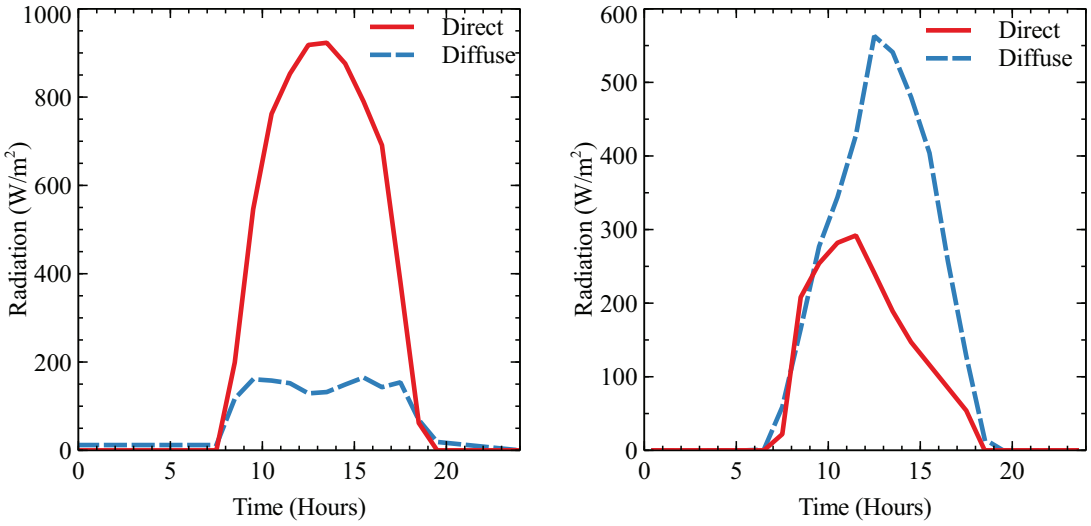

(a) Clear-sky

(b) Full cloud cover

Fig. 8: Profiles of direct and diffuse radiation for an idealized day-time scenario for two extreme situations:(a) Clear-sky and (b) Complete cloud cover

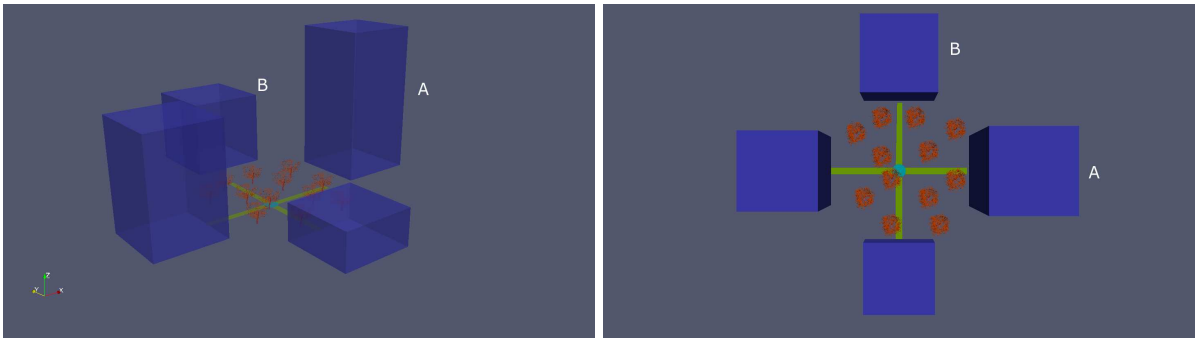

(a) Geometry Setup (b) Top View

Fig. 9: Setup of the CAD model for the idealized resolution studies. Different albedo values (given in brackets) are assigned for the pavement (0.05) - dark green , buildings (0.55) - blue , grass (0.25) - cyan, and trees (0.15) - orange. Buildings A and B are raised above the ground to create a void-deck space.

changes in the direct and diffuse radiation. This will be extremely useful real-time information during the deployment of the PV systems. Another main advantage of this approach is the ability to resolve the shadow and shading effects accurately if the solid models are available. This is demonstrated in the next section for an idealized setup.

4 Resolution Studies

To demonstrate the ability of the solar calculator to resolve shadow and shading effects accurately, two cases are considered:(a) clear-sky and (b) fully cloudy conditions. A typical distribution of the direct and diffuse solar radiation for these conditions is shown in Fig. 8. The idealized setup used for the evaluation studies is shown in Fig. 9. The setup consists of four different materials: (a) concrete (pavement and terrain), (b) paint (building), (c) greenery and (d) trees. Two of the buildings are also raised above the ground to create a void-deck space. Simulations on a coarse grid (0.25 m resolution for trees and 2 m resolution for all other surfaces) and a fine grid (0.03125 m resolution for trees and 0.25 m for all other surfaces) are performed to show the ability of the tool to resolve shadow and shading effects accurately.

The results for the clear-sky and cloudy cases on both the grids are shown in Fig. 10a-d at $\sim$ 11.30 AM in the morning. It can be clearly seen that the use of a fine mesh can better resolve the shading effects, especially for the trees. The shadow effects of trees and buildings are diffused on the coarse grids. As the solar calculator uses only surface mesh, the computations are also extremely fast (less than a minute on 64 processors for the finer mesh from 6 AM to 6 PM for a certain day). The detailed shading calculation can help in accurately placing the PV systems in urban areas.

5 Conclusions

A solar power prediction tool for urban areas was proposed by combining the numerical weather prediction model WRF with the solar load calculator in the numerical toolbox OpenFOAM. The tool was demonstrated for a residential town in the central region of Singapore. The initial results clearly show that the importance of using finer grids in WRF and accounting for solar radiation losses using urban canopy information.

This work was designed as a proof of concept study for solar power prediction using hybrid models. Extensive validation and verification of the proposed method are required in future studies. Similarly, the building and tree extrusion tool were used to demonstrate the possibility of using online data and open-source tools to provide a reasonable representation of urban canopy. These methods can be extended

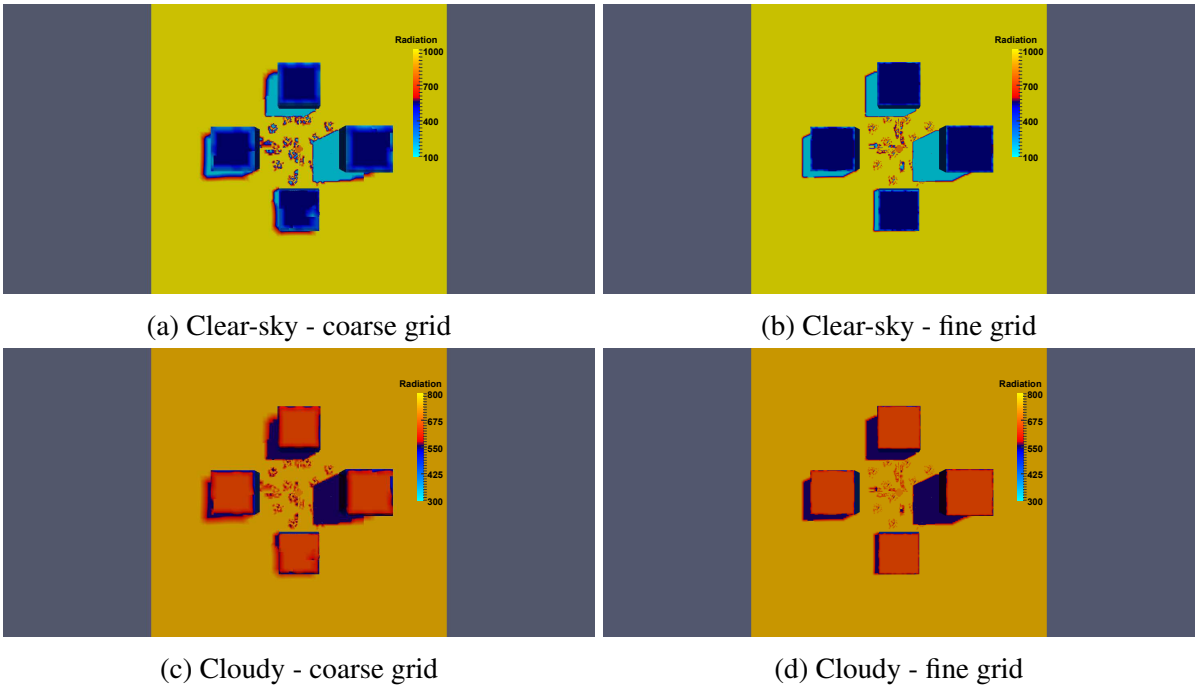

(a) Clear-sky - coarse grid

(b) Clear-sky - fine grid

(c) Cloudy - coarse grid

(d) Cloudy - fine grid

Fig. 10: Shadow and shading effects for clear-sky and fully cloudy conditions. View is from the top

further using more advanced geometry modeling libraries available for python. The developed tool will be available in the GitHub repository https://github.com/venugopalansgr/urb-solar.

Acknowledgements

The second author acknowledges the helpful discussion with Jeff Mirocha from Lawrence Livermore National Lab regarding WRF simulations. The building and tree shape creation algorithm used code from https://github.com/sebastianbeyer/concavehull/blob/master/ConcaveHull.py. Scikit-learn was used for k-means calculations. All the simulations were performed on the computer resources provided by A*CRC. The solid model in Fig. was was created using SketchUp. Post-processing was performed using python, Inkscape, Matplotlib and ParaView.

References

[1] Farmer, J. D., and Lafond, F., 2016. "How predictable is technological progress?". *Research Policy,* **45**(3), pp. 647–665.

[2] Fu, R., Feldman, D. J., Margolis, R. M., Woodhouse, M. A., and Ardani, K. B., 2017. *U.S. Solar Photovoltaic System Cost Benchmark: Q1 2017*. Sep.

[3] Reikard, G., 2009. "Predicting solar radiation at high resolutions: A comparison of time series forecasts". *Solar Energy,* **83**(3), pp. 342–349.

[4] Kemmoku, Y., Orita, S., Nakagawa, S., and Sakakibara, T., 1999. "Daily insolation forecasting using a multi-stage neural network". *Solar Energy,* **66**(3), pp. 193–199.

[5] Sfetsos, A., and Coonick, A., 2000. "Univariate and multivariate forecasting of hourly solar radiation with artificial intelligence techniques". *Solar Energy,* **68**(2), pp. 169–178.

[6] Mellit, A., Benghanem, M., and Kalogirou, S. A., 2006. "An adaptive wavelet-network model for forecasting daily total solar-radiation". *Applied Energy,* **83**(7), pp. 705–722.

[7] Pierro, M., Bucci, F., De Felice, M., Maggioni, E., Perotto, A., Spada, F., Moser, D., and Cornaro,

C., 2017. “Deterministic and stochastic approaches for day-ahead solar power forecasting”. *Journal of Solar Energy Engineering,* **139**(2), p. 021010.

[8] Perez, R., Kivalov, S., Schlemmer, J., Hemker, K., Renné, D., and Hoff, T. E., 2010. “Validation of short and medium term operational solar radiation forecasts in the us”. *Solar Energy,* **84**(12), pp. 2161–2172.

[9] Hammer, A., Heinemann, D., Lorenz, E., and Lückehe, B., 1999. “Short-term forecasting of solar radiation: a statistical approach using satellite data”. *Solar Energy,* **67**(1), pp. 139–150.

[10] Chow, C. W., Urquhart, B., Lave, M., Dominguez, A., Kleissl, J., Shields, J., and Washom, B., 2011. “Intra-hour forecasting with a total sky imager at the uc san diego solar energy testbed”. *Solar Energy,* **85**(11), pp. 2881–2893.

[11] Lorenz, E., Hurka, J., Heinemann, D., and Beyer, H. G., 2009. “Irradiance forecasting for the power prediction of grid-connected photovoltaic systems”. *IEEE Journal of selected topics in applied earth observations and remote sensing,* **2**(1), pp. 2–10.

[12] Lara-Fanego, V., Ruiz-Arias, J., Pozo-Vázquez, D., Santos-Alamillos, F., and Tovar-Pescador, J., 2012. “Evaluation of the wrf model solar irradiance forecasts in andalusia (southern spain)”. *Solar Energy,* **86**(8), pp. 2200–2217.

[13] Mathiesen, P., and Kleissl, J., 2011. “Evaluation of numerical weather prediction for intra-day solar forecasting in the continental united states”. *Solar Energy,* **85**(5), pp. 967–977.

[14] Diagne, M., David, M., Lauret, P., Boland, J., and Schmutz, N., 2013. “Review of solar irradiance forecasting methods and a proposition for small-scale insular grids”. *Renewable and Sustainable Energy Reviews,* **27**, pp. 65–76.

[15] Cao, J. C., and Cao, S., 2006. “Study of forecasting solar irradiance using neural networks with preprocessing sample data by wavelet analysis”. *Energy,* **31**(15), pp. 3435–3445.

[16] Ji, W., and Chee, K. C., 2011. “Prediction of hourly solar radiation using a novel hybrid model of arma and tdnn”. *Solar Energy,* **85**(5), pp. 808–817.

[17] Cao, S., and Cao, J., 2005. “Forecast of solar irradiance using recurrent neural networks combined with wavelet analysis”. *Applied Thermal Engineering,* **25**(2), pp. 161–172.

[18] Aryaputera, A. W., Yang, D., and Walsh, W. M., 2015. “Day-ahead solar irradiance forecasting in a tropical environment”. *Journal of Solar Energy Engineering,* **137**(5), p. 051009.

[19] Skamarock, W. C., Klemp, J. B., Dudhia, J., Gill, D. O., Barker, D. M., Duda, M. G., Huang, X.-Y., Wang, W., and Powers, J. G., 2008. A description of the advanced research wrf version 3. Tech. Rep. NCAR Tech. Note NCAR/TN-475+STR, National Center for Atmospheric Research.

[20] Weller, H. G., Tabor, G., Jasak, H., and Fureby, C., 1998. “A tensorial approach to computational continuum mechanics using object-oriented techniques”. *Computers in physics,* **12**(6), pp. 620–631.

[21] MacQueen, J., et al., 1967. “Some methods for classification and analysis of multivariate observations”. In Proceedings of the fifth Berkeley symposium on mathematical statistics and probability, Vol. 1, Oakland, CA, USA, pp. 281–297.

[22] Pedregosa, F., Varoquaux, G., Gramfort, A., Michel, V., Thirion, B., Grisel, O., Blondel, M., Prettenhofer, P., Weiss, R., Dubourg, V., Vanderplas, J., Passos, A., Cournapeau, D., Brucher, M., Perrot, M., and Duchesnay, E., 2011. “Scikit-learn: Machine learning in Python”. *Journal of Machine Learning Research,* **12**, pp. 2825–2830.

[23] Rousseeuw, P. J., 1987. “Silhouettes: a graphical aid to the interpretation and validation of cluster analysis”. *Journal of computational and applied mathematics,* **20**, pp. 53–65.

[24] Andrew, A. M., 1979. “Another efficient algorithm for convex hulls in two dimensions”. *Information Processing Letters,* **9**(5), pp. 216–219.

[25] Edelsbrunner, H., Kirkpatrick, D., and Seidel, R., 1983. “On the shape of a set of points in the plane”. *IEEE Transactions on information theory,* **29**(4), pp. 551–559.

[26] National Centers for Environmental Prediction, National Weather Service, NOAA, U.S. Department of Commerce, 2000. Ncep fnl operational model global tropospheric analyses, continuing from july 1999.

[27] Thompson, G., and Eidhammer, T., 2014. "A study of aerosol impacts on clouds and precipitation development in a large winter cyclone". *Journal of the Atmospheric Sciences,* **71**(10), pp. 3636–3658.

[28] Grell, G. A., and Freitas, S. R., 2014. "A scale and aerosol aware stochastic convective parameterization for weather and air quality modeling". *Atmos. Chem. Phys,* **14**(10), pp. 5233–5250.

[29] Iacono, M. J., Delamere, J. S., Mlawer, E. J., Shephard, M. W., Clough, S. A., and Collins, W. D., 2008. "Radiative forcing by long-lived greenhouse gases: Calculations with the aer radiative transfer models". *Journal of Geophysical Research: Atmospheres,* **113**(D13).

[30] Hong, S.-Y., Noh, Y., and Dudhia, J., 2006. "A new vertical diffusion package with an explicit treatment of entrainment processes". *Monthly Weather Review,* **134**(9), pp. 2318–2341.

[31] Jiménez, P. A., and Dudhia, J., 2012. "Improving the representation of resolved and unresolved topographic effects on surface wind in the wrf model". *Journal of Applied Meteorology and Climatology,* **51**(2), pp. 300–316.

[32] Niu, G.-Y., Yang, Z.-L., Mitchell, K. E., Chen, F., Ek, M. B., Barlage, M., Kumar, A., Manning, K., Niyogi, D., Rosero, E., et al., 2011. "The community noah land surface model with multiparameterization options (noah-mp): 1. model description and evaluation with local-scale measurements". *Journal of Geophysical Research: Atmospheres,* **116**(D12).

[33] Yang, Z.-L., Niu, G.-Y., Mitchell, K. E., Chen, F., Ek, M. B., Barlage, M., Longuevergne, L., Manning, K., Niyogi, D., Tewari, M., et al., 2011. "The community noah land surface model with multiparameterization options (noah-mp): 2. evaluation over global river basins". *Journal of Geophysical Research: Atmospheres,* **116**(D12).

[34] Jimenez, P. A., Hacker, J. P., Dudhia, J., Haupt, S. E., Ruiz-Arias, J. A., Gueymard, C. A., Thompson, G., Eidhammer, T., and Deng, A., 2016. "Wrf-solar: Description and clear-sky assessment of an augmented nwp model for solar power prediction". *Bulletin of the American Meteorological Society,* **97**(7), pp. 1249–1264.

[35] The OpenFOAM Foundation Ltd. Openfoam v5.0. www.openfoam.org.

[36] OpenCFD Ltd. Openfoam v1612. www.openfoam.com.

[37] Klucher, T. M., 1979. "Evaluation of models to predict insolation on tilted surfaces". *Solar energy,* **23**(2), pp. 111–114.

[38] Maxwell, E. L., Stoffel, T. L., and Bird, R. E., 1986. Measuring and modeling solar irradiance on vertical surfaces. Tech. rep., Solar Energy Research Inst., Golden, CO (USA).

[39] Pomeroy, J. W., Marks, D., Link, T., Ellis, C., Hardy, J., Rowlands, A., and Granger, R., 2009. "The impact of coniferous forest temperature on incoming longwave radiation to melting snow". *Hydrological processes,* **23**(17), pp. 2513–2525.

[40] Kubilay, A., Derome, D., and Carmeliet, J., 2017. "Coupling of physical phenomena in urban microclimate: A model integrating air flow, wind-driven rain, radiation and transport in building materials". *Urban Climate*.